The Peak Overpressure Field Resulting From Shocks Emerging From Circular Shock Tubes

A. J. Newman
Mechanical and Aerospace Engineering,
SUNY,
302 Jarvis Hall,
Buffalo, NY 14260-4400
e-mail: ajnewman@buffalo.edu

J. C. Mollendorf
Professor
Mechanical and Aerospace Engineering,
SUNY,
335 Jarvis Hall,
Buffalo, NY 14260-4400
e-mail: molendrf@buffalo.edu

A simple semi-empirical model for predicting the peak overpressure field that results when a shock emerges from a circular shock tube is presented and validated. By assuming that the shape of the expanding shock remains geometrically similar after an initial development period, an equation that describes the peak overpressure field in the horizontal plane containing the shock tube's centerline was developed. The accuracy of this equation was evaluated experimentally by collecting peak overpressure field measurements along radials from the shock tube exit at 0 deg, 45 deg, and 90 deg over a range of shock Mach numbers from 1.15 to 1.45. It was found that the equation became more accurate at higher Mach numbers with percent differences between experimental measurements and theoretical predictions ranging from 1.1% to 3.6% over the range of Mach numbers considered. (1) Shocks do propagate in a geometrically similar manner after some initial development length over the range of Mach numbers considered here. (2) The model developed here gives reasonable predictions for the overpressure field from a shock emerging from a circular shock tube. (3) Shocks are expected to be completely symmetric with respect to the shock tube's centerline, and hence, a three dimensional overpressure field may be predicted by the model developed here. (4) While there is a range of polar angle at which the shock shape may be described as being spherical with respect to the shock tube's exit, this range does not encompass the entirety of the half space in front of the shock tube, and the model developed here is needed to accurately describe the entire peak overpressure field. [DOI: 10.1115/1.4002183]

Keywords: shock tube, pressure field, semi-empirical

1 Introduction

A simple semi-empirical model for predicting the peak overpressure field that results when a shock emerges from a circular shock tube is presented and validated. Blast waves were generated using an open-ended shock tube, and the goal was to describe the blast wave peak overpressure field in terms of shock tube parameters and spatial geometry. The physical situation under consideration is shown in Fig. 1.

This pressure field has been previously studied experimentally by Bertrand and Matthews [1] and by Sloan and Nettleton [2]. Bertrand and Matthews [1] collected side-on pressure measurements of the peak pressure fields, which resulted when open-ended shock tubes of inside diameters of 56.4 cm, 20.3 cm, 11.4 cm, and 4.8 cm (22.1875 in., 8 in., 4.5 in., and 1.875 in.) were discharged. Three of these shock tubes were cold gas driven, and one was detonation driven. They observed that all plots of peak overpressure versus distance along the 90 deg radial (see Fig. 1(b)) had approximately the same slope. Based on this observation, an empirical equation was proposed that described the peak overpressure decay along the 90 deg radial. Sloan and Nettleton [2] conducted experiments using a closed-end shock tube with a sudden change in cross sectional area (from 79 mm to 1 m) to model an expanding shock in half space ($0 \le \theta \le 180$ in Fig. 1(b)). They collected face-on pressure measurements along the 90 deg radial (see Fig. 1(b)) at varying distances from the sudden area change. They compared these with a theoretical model that they proposed for the peak overpressure decay along the 90 deg radial based on the theory of Skews [3,4], Whitham [5,6], and Chisnell

[7]. While both models 1 and 2 compared well with their respective experimental data, Bertrand and Matthews' [1] is more applicable to the current research since it was also for open-ended shock tubes. As stated, Sloan and Nettleton's [2] was for half space. The diffracting shock theory put forth by Whitham [5,6] can also be directly applied to the current situation. In addition to peak overpressure field, several other aspects of open-ended shock tube flows have been previously studied. Rather than list these references here, the interested reader is referred to Haselbacher et al. [8] and Newman [9], which both contain a more exhaustive list of research relating to open-ended shock tube flows in general.

The approach taken in the presently reported research is to (1) use the theory of Whitham [5,6] to predict the evolving shape of the shock wave, (2) assume that shocks propagate in a geometrically similar manner after some initial development length, (3) determine a mathematical function for the geometrically similar expanding wave's shape, and (4) relate this function to shock tube parameters and peak overpressure field using a method similar to that of Bertrand and Matthews [1].

2 Analysis

Neglecting the wall thickness of the shock tube, Whitham's [5,6] diffracting shock theory can be easily applied to the presently reported research to predict the shape of a fully developed shock. The format for this is shown in Fig. 2.

It is clear in Fig. 2 that in any plane containing the shock tube's centerline, the shock is axisymmetric with respect to the shock tube's centerline. It is assumed that this symmetry is maintained as the shock expands. It is common in literature [2,10] to take the emerging shock to be developing until the most inner characteristic curves of the expansion fan located on the shock tube's edge
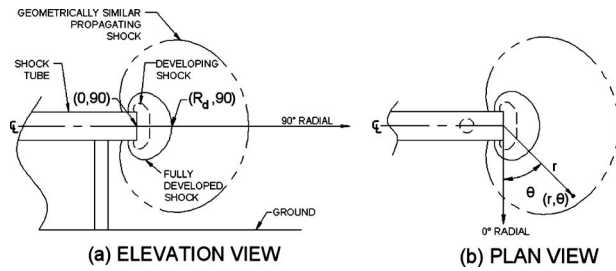
Fig. 1 Physical situation considered here. Shown above is the emerging shock at three stages: developing, developed, and when the shock propagates in a geometrically similar manner. The polar coordinate system is shown in the plan view (*b*). Spatial points labeled in the elevation view (*a*) along the 90 deg radial are 0 at the opening of the shock tube and R_d, where the shock becomes fully developed.

meet at the shock tube's centerline (see Fig. 2). The distance along the 90 deg radial at which this occurs is called the development length, denoted as R_d (see Fig. 1(*a*)).

Skews [3,4] also gave a method for calculating R_d; however, the methods of both Whitham [5,6] and Skews [3,4] were shown by Sloan and Nettleton [2] to significantly overestimate R_d when compared with their own experimental data. It is critical to know this length so that the range of validity of the equation to be developed is known. Skews' [3,4] method was shown to typically give results closer to those observed by Sloan and Nettleton [2] for development length. Therefore, Skews' [3,4] theory was used to offer a conservative estimate for the lower bound of the range of validity; the equation being developed is not expected to be valid within a circle of radius R_d centered at $r=0$ (see Fig. 1(*b*)). Development lengths predicted by Skews' [3,4] theory for the range of shock Mach numbers covered in this research are given in Table 1 in nondimensional form.

It was observed that in the half space in front of the shock tube, the shape of the fully developed shock, as calculated by Whitham's [5,6] theory, could be closely approximated by a cardioid (see Fig. 3). The shape of the cardioid deviates from the shape calculated from Whitham's [5,6] theory in regions behind the shock tube's exit, but these regions are not of interest in the current study.

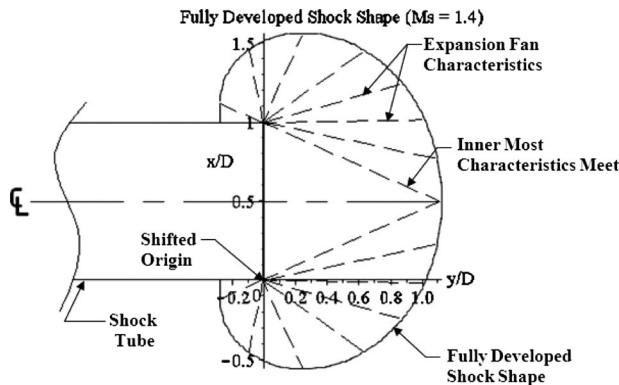In polar coordinates, a cardioid has an equation of the form

Fig. 2 Fully developed shock shape. Shown above is the typical shape of a fully developed shock emerging from the shock tube used in the current research as calculated by Whitham's theory [5] (p. 161) for $M_s=1.41$. The view shown above is the plan view. The *x* axis indicates distance in meters from the shock tube exit along the 0 deg radial, and *y* indicates distance in meters along the 90 deg radial. Note, however, the shift in origin from the shock tube centerline to the edge. This is done to facilitate wave shape calculation.

Table 1 Development lengths for shocks emerging from a shock tube as predicted by Skews' [3,4] theory for the range of M_s considered here

M_s	Development length R_d/D
1.15	1.13
1.20	1.06
1.29	0.98
1.35	0.94
1.41	0.93
1.45	0.92

$$r = a + b \sin(\theta) \qquad (1)$$

In Eq. (1), we take r as the radial distance from the shock tube exit's center and θ as the polar angle (as in Fig. 1(*b*)). Assumptions are next made about the parameters a and b to relate peak overpressure and distance. Since for $\theta=0$, $r=a$, it follows that a must give the peak overpressure-distance relation along the 0 deg radial. By a similar argument, for $\theta=90$, $r=a+b$, and $a+b$ must give the peak overpressure-distance relation along the 90 deg radial. It is physically clear that peak overpressure must decrease with increasing distance from the shock source. Experimental peak overpressure versus distance data presented in literature [1–3,7] indicates that the relation is a power law. Therefore, the general form of a and $a+b$ will be

$$a, a+b = \frac{k}{P^\alpha} \qquad (2)$$

Indirectly, a form of this type for $a+b$ was proposed by Bertrand and Matthews [1]. They noted that the pressure-distance relation on the centerline for all M_s they considered (0.90–1.26) was

$$P(r,90) = P_{90}\left(\frac{R_{90}}{r}\right)^{1.12} \qquad (3)$$

where the exponent of 1.12 was determined experimentally.

Rearranging Eq. (3),

$$r = R_{90}\left(\frac{P_{90}}{P(r,90)}\right)^{0.89} = a + b \qquad (4)$$

Since Bertrand and Matthews [1] determined that the exponent along the 90 deg radial was constant for the range of M_s they considered, the same was assumed in the current research for the 0 deg radial. By collecting peak overpressure measurements along the 0 deg radial for *one* fixed M_s (1.35), a was found to vary as
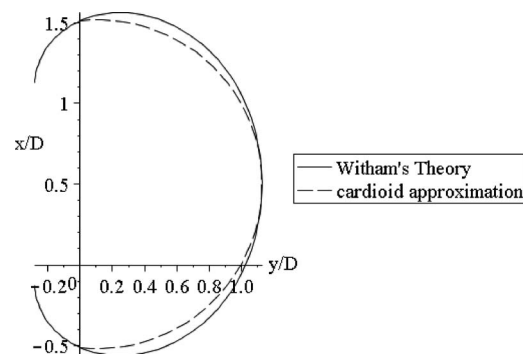

Fig. 3 Shown above is a comparison between the shape of the fully developed shock wave as calculated by the authors using Whitham's [5] (p. 161) theory and the shape of the fully developed shock described using the equation of a cardioid
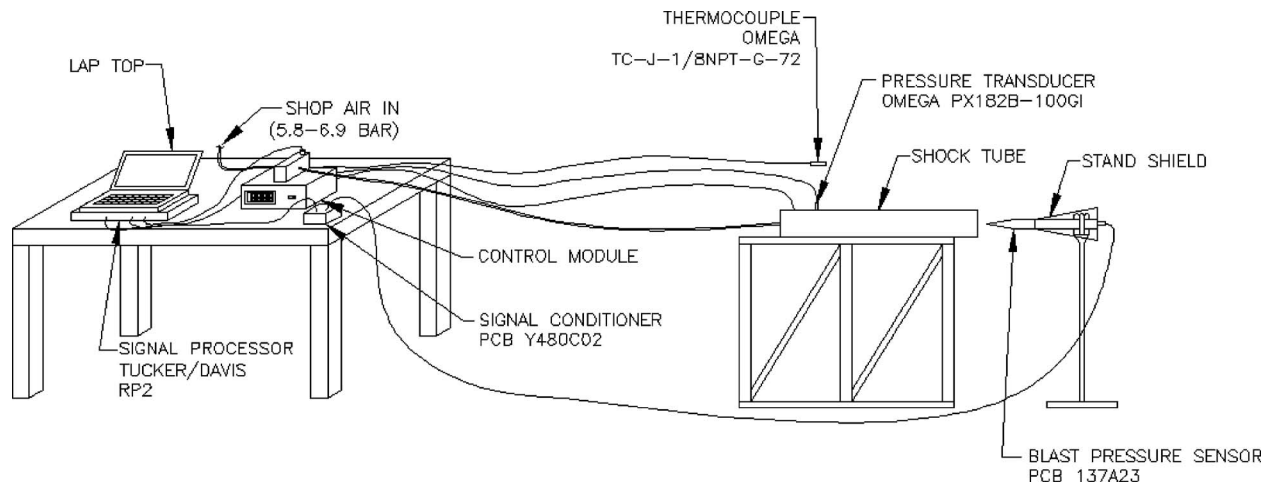
Fig. 4 Experimental setup schematic detailing the major components of peak overpressure measurement experiments

$$a = R_0 \left(\frac{P_0}{P(r,0)} \right)^{0.97} \tag{5}$$

Now, Eqs. (4) and (5) are used with Eq. (1) so that for $\theta = 90$, 0 Eq. (1) reduces to Eqs. (4) and (5), respectively.

Therefore,

$$r = R_0 \left(\frac{P_0}{P(r,\theta)} \right)^{0.97} + \left[R_{90} \left(\frac{P_{90}}{P(r,\theta)} \right)^{0.89} - R_0 \left(\frac{P_0}{P(r,\theta)} \right)^{0.97} \right] \sin(\theta) \tag{6}$$

Equation (6), also called the cardioid approximation here, gives the peak overpressure field implicitly as a function of shock tube parameters and spatial geometry. Shock tube parameters enter into Eq. (6) implicitly through the reference points along the 0 deg and 90 deg radials: R_0, R_{90}, P_0, and P_{90}.

3 Experimental Validation

To assess the accuracy of the cardioid approximation, peak overpressure measurements were collected along the 0 deg, 45 deg, and 90 deg radials (see Fig. 1(b)) at nondimensional distances (r/D) between 2.9 and 19.5. It can be seen in Table 1 that all measurements were collected outside of the development region. A schematic of the experimental setup used to generate shocks and collect peak overpressure data is shown in Fig. 4.

Shocks were produced using an in-house-built 5.21 cm (2 in.) internal diameter, diaphragm equipped, open-ended shock tube. Lengths of the shock tube's driver and driven sections were approximately 0.81 m and 0.38 m (32 in. and 15 in.), respectively. Air was used for both the driver and driven gases. Diaphragms used were glued multilayered aluminum foil with thicknesses ranging from approximately 0.13 mm to 1.4 mm (5–55 mil). Diaphragms were ruptured using a solenoid actuated hunting arrow. Details can be found in Ref. [9].

Shock tube driver pressure (gauge) and ambient temperature readings were collected by the control module connected to an Omega PX182B-100GI flush mounted pressure transducer and an Omega TC-J-1/8NPT-G-72 thermocouple. It both displayed their values on a digital readout and transmitted them to the laptop by way of an Omega DPi32-C24 process monitor housed within. In addition to the functions just mentioned, the control module was also used to regulate the shock tube driver pressure using an Omega IP610-X30 electronic air pressure controller and to fire the shock tube using a low voltage transistor switch.

To conduct an experiment, a new diaphragm would be placed in the shock tube, and then a MATLAB code running on the laptop would be executed. This code used desired shock tube driver pressure in psia, diaphragm material and number of layers, time duration of data collection, polar angle, and radial distance as inputs. Once this information was entered, MATLAB would interface with DPi32-C24 to monitor pressure. MATLAB also opened the RPVDSEX (Tucker/Davis O.S.) code on the Tucker/Davis RP2 signal processor, which collected data, regulated pressure, and fired the shock tube. The shock tube driver pressure supplied by either shop air or portable compressor rapidly increased to 75% of the desired value and then increased slowly to 100%. When the shock tube driver pressure was detected by MATLAB (continuously monitoring output from DPi32-C24) to be at the desired value, it would pass a parameter to the RPVDSEX code, signaling it to begin collecting data from the PCB piezotronics 137A23 blast probe and Y480C02 signal conditioner. Immediately following this, a signal was sent to the main control module, which fired the shock tube. After it had been fired, the shock tube driver pressure was set to zero, which stopped the air flow.

Data collected were then transmitted to MATLAB where it was displayed as a voltage versus time signature. A typical voltage-time signature is shown in Fig. 5(a). It is known that blast probes of the type used in the current research have an inherent overshoot so that the actual peak overpressure is not the displayed peak. To find the true peak overpressure, it is necessary to use an exponential least-squares fit over a portion of the positive phase and to extrapolate back to the shock arrival time [11]. An example of this is shown in Fig. 5(b).

Comparisons between experimental measurements of the peak overpressure ratio and theoretical predictions are shown for the range of M_s as functions of r/D in Figs. 6(a)–6(f). The experimental uncertainty in these measurements is slightly greater than
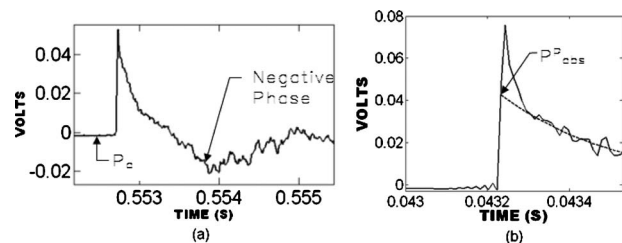

Fig. 5 Typical voltage/time signature. Clearly visible are the peak overpressure and the negative phase characteristic of blast waves. The above figures are for a fixed point in space. P^P_{abs} is the maximum pressure reached at the point when the blast wave passes determined by using an exponential least-squares fit over a portion of the positive phase extrapolated back to the shock arrival time. The negative phase represents the effects of the following rarefaction wave at the point.
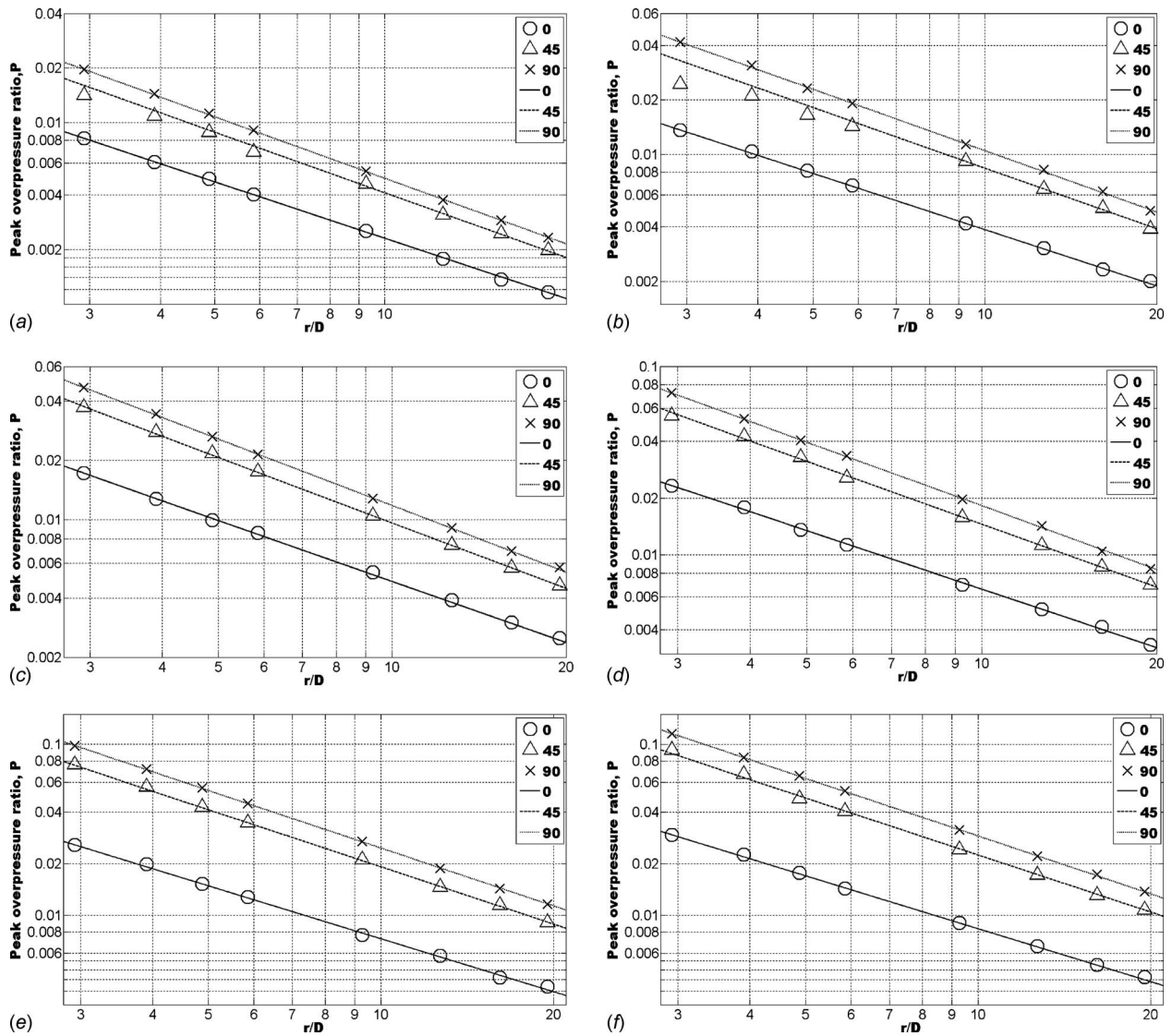
Fig. 6 (*a*) Comparison of experimental data (symbols) and theoretical predictions using Eq. (6) (lines) along the 0 deg, 45 deg, and 90 deg radials for $M_s = 1.15$. (*b*) Comparison of experimental data (symbols) and theoretical predictions using Eq. (6) (lines) along the 0 deg, 45 deg, and 90 deg radials for $M_s = 1.20$. (*c*) Comparison of experimental data (symbols) and theoretical predictions using Eq. (6) (lines) along the 0 deg, 45 deg, and 90 deg radials for $M_s = 1.29$. (*d*) Comparison of experimental data (symbols) and theoretical predictions using Eq. (6) (lines) along the 0 deg, 45 deg, and 90 deg radials for $M_s = 1.35$. (*e*) Comparison of experimental data (symbols) and theoretical predictions using Eq. (6) (lines) along the 0 deg, 45 deg, and 90 deg radials for $M_s = 1.41$. (*f*) Comparison of experimental data (symbols) and theoretical predictions using Eq. (6) (lines) along the 0 deg, 45 deg, and 90 deg radials for $M_s = 1.45$.

1%. The 137A23 blast probe has a linearity of $\pm 0.1\%$ FS, which equals 0.0996 mV/psi, and the Y480C02 signal conditioner has an accuracy of $\pm 1\%$.

4 Discussion

As can be seen in Figs. 6(*a*)–6(*f*), predictions made by Eq. (6) agree quite well both qualitatively and quantitatively with the experimental data collected.

In Fig. 6(*a*), it may be observed that theoretical predictions agree qualitatively quite well for all angles. Quantitative agreement is slightly better for the 0 deg and 90 deg radials than for the 45 deg radials. Percent differences are approximately 1.1%, 4.2%, and 0.7% for the 0 deg, 45 deg, and 90 deg radials, respectively.

A behavior similar to that noted in Fig. 6(*a*) is also observed in Fig. 6(*b*). The percent differences along the 0 deg, 45 deg, and 90 deg radials are approximately 1.4%, 8.1%, and 1.2%.

In Figs. 6(*c*)–6(*f*), experimental data are seen to agree with theoretical predictions quite well. Average percent differences were 1.1%, 1.3%, 1.2%, and 1.3%, respectively. No notable deviations are observed. Average and individual radial percent differences for each M_s are summarized in Table 3 and Fig. 7.

In the construction of the theoretical peak overpressure ratio versus r/D curves, the reference points along the 0 deg and 90 deg radials used in Eq. (6) were those collected at the lowest value of r/D (see Table 2).

This point is worth emphasizing since it illustrates the power of Eq. (6). The theoretical curves shown in Figs. 6(*a*)–6(*f*) were based only on *two* experimentally measured points, one on the 90 deg radial and one on the 0 deg radial. 45 deg curves are generated without any experimental measurements. The selection of reference points is arbitrary so long as both points are collected at the same r/D. If reference points not taken at the same r/D value are used, the cardioid approximation will still provide reasonable

Table 2 Shown here are the reference points used in Eq. (6) for the construction of the theoretical peak overpressure ratio versus r/D curves shown in Figs. 6(a)–6(f)

M_s	P_0	r/D_0	P_{90}	r/D_{90}
1.15	0.0082	2.93	0.0196	2.93
1.2	0.0137	2.93	0.0418	2.93
1.29	0.0172	2.93	0.0470	2.93
1.35	0.0233	2.93	0.0726	2.93
1.41	0.0258	2.93	0.0982	2.93
1.45	0.0295	2.93	0.1156	2.93

Fig. 8 Shown above is the effect that choice of reference point has on the cardioid approximation. One set of predictions is made using the first data point (lowest r/D value), one uses the fourth data point, and one uses the last data point (highest r/D value).
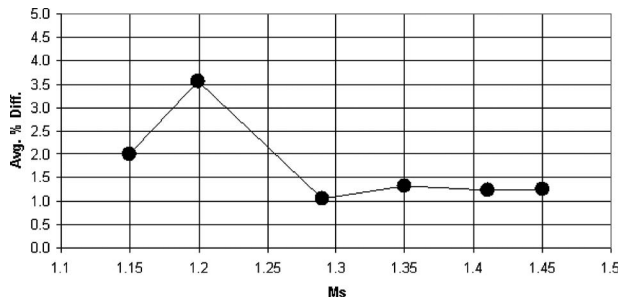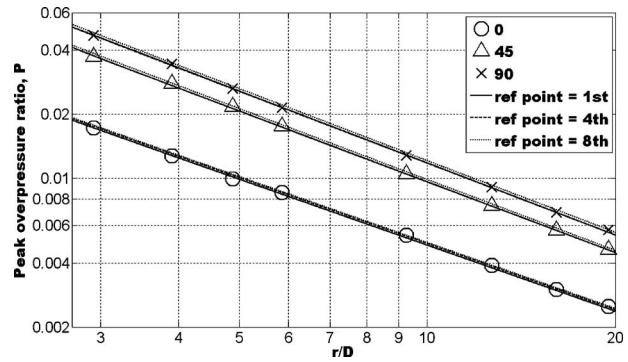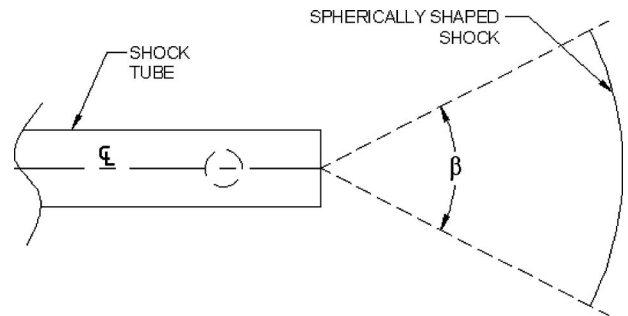

Fig. 7 Average percent differences between experimental measurements and theoretical predictions as a function of M_s. A general trend of decreasing percent difference with increasing M_s is clearly visible.

Fig. 9 Based on the data, it is apparent that there is a certain range of polar angle, labeled β above, for which the wave shape may be accurately described as being spherical with respect to the shock tube exit. A detailed treatment of spherical shocks of this nature is given in Ref. [2].

Table 3 Average percent differences between experimental data and theoretical predictions for the range of M_s

M_s	Percent diff.

M_s	0 deg	45 deg	90 deg	Avg.
1.15	1.1	4.2	0.7	2.0
1.2	1.4	8.1	1.2	3.6
1.29	1.7	0.8	0.7	1.1
1.35	1.4	1.5	1.1	1.3
1.41	2.0	1.1	0.6	1.2
1.45	1.4	1.8	0.6	1.3

estimates for the peak overpressure field, but the accuracy will decrease. A visual comparison of the effect of reference point choice is given in Fig. 8 for $M_s=1.29$; the behavior shown is typical of all values of M_s examined.

It can be seen visually in Figs. 6 and 7 and quantitatively in Table 3 that the cardioid approximation improves with increasing M_s. In Fig. 6, the experimental data maintain a tighter spread around the theoretical predictions with increasing M_s, and average percent differences shown in Table 3 generally decrease with increasing M_s. It may also be observed that there is a relatively large
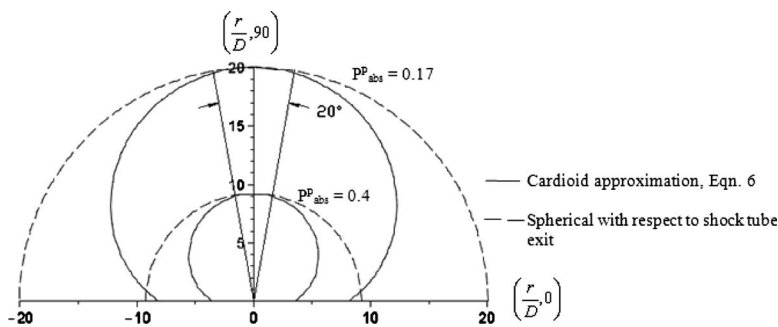

Fig. 10 Plot of isobars predicted by Eq. (6) and isobars given by assuming spherical shape both for $M_s=1.41$. At this value of shock Mach number, for the value for β shown above, the percent difference between isobars predicted by the cardioid approximation and isobars from assuming a spherical shape ranges between 0% (at 90 deg) and 4% (at 80 deg and 100 deg). These values are typical for the range of M_s considered here.
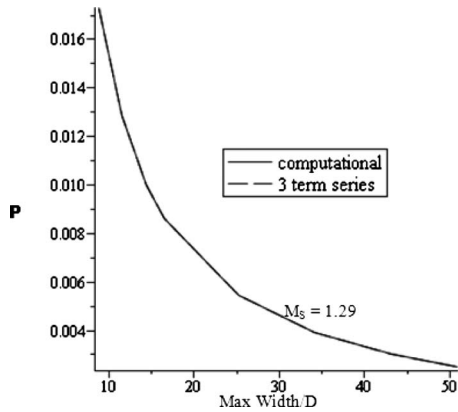
Fig. 11 P versus max width/D for $M_s=1.29$. The difference between values calculated using the computational solution of Eq. (8) and the perturbation solution (Eq. (9)) are virtually indistinguishable. Agreement between computational and perturbation solutions are equally as good for the range of M_s considered here.

jump in accuracy of the cardioid approximation for a small change in M_s (percent difference changes from 3.6 to 1.1 for a change in M_s from 1.2 to 1.29).

Since the experimental data and theoretical predictions agree well for the range of M_s considered and over the range of distances at which data were collected, it may be concluded that the shape of the wave in these regions is, in fact, a cardioid with origin at the shock tube exit. There is, however, a range of polar angles for which the wave shape may be approximated as being spherical with respect to the shock tube exit (see Fig. 9). Analyses involving the range of polar angles over which the wave may be approximated as being spherical were conducted by Sloan and Nettleton [2]. A qualitative analysis of the size of the region in which the wave may be approximated as being spherical with respect to the shock tube exit is given in Fig. 10. From this figure, it may be seen that a spherical approximation is valid for only about 9% of the total polar angle covered by the pressure field.

Another benefit of the cardioid approximation is that the maximum width of the expanding shock may be easily calculated as a function of peak overpressure. From Eq. (6), the x coordinate in the Cartesian coordinates may be given as

$$x = R_0 \cos(\theta) \cdot \left(\frac{P_0}{P(r,\theta)} \right)^{0.97} + \left(\frac{1}{2} \right) \cdot \left[R_{90} \left(\frac{P_{90}}{P(r,\theta)} \right)^{0.89} \right.$$

$$\left. - R_0 \left(\frac{P_0}{P(r,\theta)} \right)^{0.97} \right] \sin(2\theta) \qquad (7)$$

Maximizing Eq. (7) for θ leads to the equation

$$\frac{\cos(2\theta)}{\sin(\theta)} = \zeta \qquad (8)$$

where

$$\zeta = \frac{R_0 \left(\dfrac{P_0}{P} \right)^{0.97}}{R_{90} \left(\dfrac{P_{90}}{P} \right)^{0.89} - R_0 \left(\dfrac{P_0}{P} \right)^{0.97}}$$

Equation (8) may either be solved numerically or θ may be given to a good approximation by

$$\theta = \frac{\pi}{4} - \frac{1}{2\sqrt{2}} \zeta + \frac{1}{8} \zeta^2 \qquad (9)$$

Using Eqs. (9) and (7), the maximum width of the shock wave is known as a function of peak overpressure only (see Fig. 11).
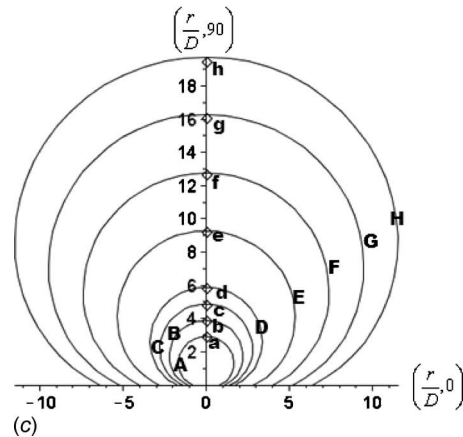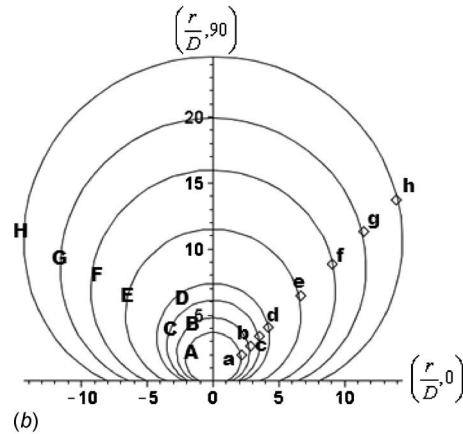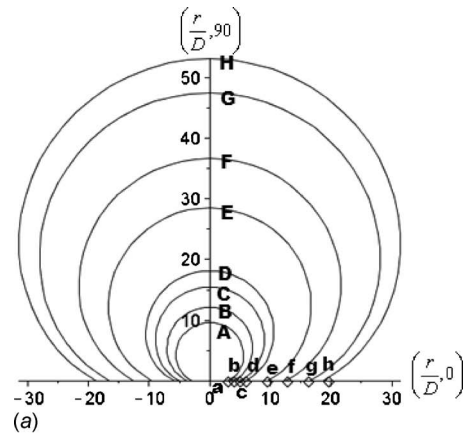

(a)

(b)

(c)

Fig. 12 (a) Comparison of experimental data points on the 0 deg radial (symbols labeled in lower case letters) and the isobars of identical peak overpressure predicted by the cardioid approximation (labeled in capital letters). Axes are scaled distances (r/D) at 0 deg and 90 deg; the center of the shock tube's exit is located at (0,0). (b) Comparison of experimental data points (symbols labeled in lower case letters) and theoretical isobars (uppercase labels) on the 45 deg radial. (c) Comparison of experimental data points (symbols labeled in lowercase labels) and theoretical isobars (uppercase labels) on the 90 deg radial.

In addition to the comparisons given in Fig. 6, another type of comparison between the theoretical predictions and experimental measurements can be made. Equation (6) can be used to generate isobars of the expanding shock (as first shown in Fig. 10), and these may then be compared with the experimental data points. A representative comparison for $M_s=1.41$ is given in Fig. 12; simi-

lar plots can be generated for the range of M_s.

The format of the plot used in Fig. 12 provides a more complete view of the peak overpressure field, whereas those shown in Fig. 6 provide an easier visual comparison between experimental and theoretical data.

There is also an added benefit of the cardioid approximation, which has not been mentioned. In addition to assuming that the expanding shock is symmetric in the horizontal plane containing the shock tube's centerline, it can also be reasonably assumed that in the approximation's range of validity, the shock is completely symmetric about the shock tube's centerline. Therefore, it is expected that Eq. (6) can reasonably describe a three dimensional peak overpressure field.

Plots of the type featured in Figs. 6 and 12 were first presented in Ref. [9] using pilot data. Experimental data used here are new.

5 Conclusions

Based on the comparison between experimental data and theoretical predictions, several conclusions about the physical situation under current consideration may be drawn. First, shocks emerging from a circular shock tube *do* propagate in a geometrically similar manner after an initial development length over the range of Mach numbers considered here. Second, based on the comparisons given in Figs. 6 and 12 and Table 3, the cardioid approximation gives reasonable predictions for the peak overpressure field, resulting from a shock emerging from a circular shock tube. Third, shocks are expected to be completely symmetric about the shock tube's centerline (measurements were not collected to experimentally confirm this), allowing the approximation to predict a three dimensional peak overpressure field. Fourth, while there is a range of polar angles at which the shock shape may be described as being spherical with respect to the shock tube exit, this range does not encompass the entirety of the half space in front of the shock tube (see Fig. 10), and the cardioid approximation must be used to accurately describe the peak overpressure field.

Acknowledgment

Nomenclature

C_L = centerline of shock tube (Fig. 1)
D = shock tube internal diameter (cm)
M_s = shock Mach number
P = pressure (kPa (gauge))
P_n = experimental pressure measurement (kPa (gauge)) at location R_n on the n radial

P_a = atmospheric pressure (kPa (absolute))
P_{abs} = measured side-on pressure (kPa (absolute))
P = peak overpressure ratio, $(P_{abs}^P - P_a)/P_a$ (dimensionless)
R_d = shock development length (m)
R_n = experimental measurement location on the n radial (m)
a, b, c = cardioid parameters (Eqs. (1), (2), and (4)–(6))
k = a constant (Eq. (2))
r/D = nondimensional radial coordinate
r = radial coordinate (m)
x, y = Cartesian distance coordinates (m)

Greek

α = a constant (Eq. (2))
β = polar angle range of spherical shock wave
θ = angular coordinate (rad or deg)
ζ = dimensionless ratio of cardioid parameters, a/b (Eqs. (9))

Subscript

n = indicates a measurement taken on the n deg radial ($n=0$, $n=45$, etc.)

Superscript

P = peak

References

[1] Bertrand, B., and Matthews, W., 1965, "Overpressures and Durations of Shock Waves Emerging From Open-Ended Shock Tubes," U.S. Army Materiel Command Ballistic Research Laboratories, Aberdeen, MA, Memorandum Report No. 1724.
[2] Sloan, S. A., and Nettleton, M. A., 1975, "A Model for the Axial Decay of a Shock Wave in a Large Abrupt Area Change," J. Fluid Mech., **71**(4), pp. 769–784.
[3] Skews, B. W., 1966, "Profiles of Diffracting Shock Waves," Department of Mechanical Engineering, University of Witwatersand, Johannesburg, Report No. 3.
[4] Skews, B. W., 1967, "The Shape of a Diffracting Shock Wave," J. Fluid Mech., **29**(2), pp. 297–304.
[5] Whitham, G. B., 1957, "New Approach to Problems of Shock Dynamics Part 1: Two Dimensional Problems," J. Fluid Mech., **2**(2), pp. 145–171.
[6] Whitham, G. B., 1959, "A New Approach to the Problems of Shock Dynamics. Part 2. Three Dimensional Problems," J. Fluid Mech., **5**(3), pp. 369–386.
[7] Chisnell, R. F., 1957, "The Motion of a Shock Wave in a Channel With Applications to Cylindrical and Spherical Shock Waves," J. Fluid Mech., **2**(3), pp. 286–298.
[8] Haselbacher, A., Balachandar, S., and Kieffer, S., 2007, "Open-Ended Shock Tube Flows: Influence of Pressure Ratio and Diaphragm Position," AIAA J., **45**(8), pp. 1917–1929.
[9] Newman, A. J., 2010, "The Peak Overpressure Field Resulting From the Discharge of an Open-Ended Shock Tube," Mechanical and Aerospace Engineering, State University of New York at Buffalo, Buffalo, NY.
[10] Sloan, S. A., and Nettleton, M. A., 1978, "A Model for the Decay of a Wall Shock in a Large Abrupt Area Change," J. Fluid Mech., **88**(2), pp. 259–272.
[11] Walter, P. L., 2010, "Measuring Static Overpressures in Air Blast Environments," PCB Piezotronics, Depew, NY, Technical Note No. PCB-TN-27-051009.